Magnesium Technology 2012
Edited by: Suveen N. Mathaudhu, Wim H. Sillekens, Neale R. Neelameggham, and Norbert Hort
TMS (The Minerals, Metals & Materials Society), 2012

TEXTURE EVOLUTION DURING HOT DEFORMATION PROCESSING OF Mg-3Sn-2Ca-0.4Al ALLOY

C. Dharmendra[1], K.P. Rao[1], Y.V.R.K. Prasad[2], N. Hort[3], K.U. Kainer[3]

[1]Department of Mechanical and Biomedical Engineering
City University of Hong Kong, 83 Tat Chee Avenue Kowloon, Hong Kong SAR, China
[2]processingmaps.com (formerly at City University of Hong Kong, Hong Kong, China)
[3]Helmoltz-Zentrum Geesthacht, Max-Planck Str. 1, Geesthacht 21502, Germany

Keywords: Mg-Sn-Ca-Al alloy, Hot Compression, Processing Maps, EBSD, Texture

Abstract

An experimental investigation of texture evolution during high temperature compression of Mg-3Sn-2Ca (TX32) alloy containing 0.4%Al using electron back scatter diffraction (EBSD) technique is reported. Isothermal uniaxial compression tests were performed in the temperature and strain rate ranges 300-500 °C and 0.0003-10 s^{-1} to examine the influence of processing conditions on the dynamic recrystallization (DRX) behavior and texture evolution. The onset of DRX during compression at low temperatures (300 and 350 °C) and low strain rates (0.0003 and 0.001 s^{-1}) gave rise to a fine, partially recrystallized and necklaced grain microstructure, with the basal poles located at 15-30° from the compressive direction although they were split. Specimens deformed at temperatures higher than 450 °C resulted in a fully recrystallized microstructure and an almost random crystallographic texture. It is clear from Schmid factor analysis that the contribution of pyramidal slip system is significant for deformation at temperatures above 450 °C.

Introduction

Magnesium alloy products, because of their low density, high specific strength and favorable recycling capability, offer great potential for automotive and aircraft industries to replace steel and other high density materials [1]. However, a major obstacle to wider use of magnesium alloys is their poor ductility. The deformation of magnesium alloys is extremely orientation dependent due to their hexagonal close-packed (hcp) crystal structure and the availability of limited number of slip systems at room temperature. Basal slip and the tension twinning are the most readily available slip systems at room temperature [2]. In the hcp metals, the only plane with high atomic density is basal plane (0001). The plastic deformation of poly crystals requires five independent slip systems. For extensive workability in magnesium alloys, slip on (0001) basal, $(10\bar{1}0)$ prismatic and $(11\bar{2}2)$ second order pyramidal planes is essential [3]. Studies on single crystal deformation [2, 4] showed that the critical resolved shear stresses (CRSS) required for activating non-basal slip modes are considerably higher than for basal slip system. Increasing deformation temperatures decreases CRSS and thus, non-basal slip modes also activate and become more important as temperature raises. For the operation of a slip system, there are two conditions, i.e. energy condition and the geometric condition. The energy condition can be described by CRSS while the geometric condition can be described by Schmid factor. The geometric condition for a slip system to operate, under an uniaxial compression condition be expressed by Schmid's law [5]

$$T_c = \pm \sigma \cos\varphi \cos\lambda \quad (1)$$

where T_c is the critical resolved shear stress, σ is the applied stress, φ is the angle between the slip direction and compressive direction, λ is the angle between the normal direction of the slip plane and the compressive direction. The Schmid factor is defined as $m = \cos\varphi \cos\lambda$. For a given slip system with a CRSS T_c, the required yield stress is determined by the Schmid factor 'm' or the crystallographic orientation of the grain, with small Schmid factor being unfavorable for slip to operate.

Magnesium develops strong textures during processing and affects the ductility of Mg-based alloys [6]. In practice, ductility can be improved by working at elevated temperatures [7], finer grain sizes and solute additions [8]. All of these can be rationalized in terms of non-basal slip activation [9]. As-cast and wrought materials both differ in grain size and texture, factors which are known for a strong influence on deformation behavior of magnesium alloys even at high temperatures.

Along with ductility, good corrosion and creep resistance properties are also significant to employ the magnesium alloys as structural materials. To improve these properties, newer Mg-Sn-Ca (TX series) alloys are being developed and the studies of some Mg-Sn-Ca alloys indicate reasonable corrosion and good creep resistance, particularly Mg-3Sn-2Ca (TX32) alloy has exhibited good creep resistance [10-12]. Aluminum addition improves room temperature mechanical properties of Mg by solid solution strengthening due to large atomic size difference (16%) and also precipitation of (β-$Mg_{17}Al_{12}$) intermetallic phase [13]. However, 0.4 wt% Al to the Mg-3Sn-2Ca alloy does not cause the formation of any new phases. Keeping that in view, 0.4 wt% Al was added to TX32 alloy. Alloying additions can alter the deformation mechanisms, which in turn influence the texture. The aim of the present work is to study the hot compressive deformation behavior of Mg-3Sn-2Ca-0.4Al alloy in as-cast condition using the processing map technique and to evaluate the development of microstructures and micro-textures in the deformed specimens using SEM based EBSD technique. The *processing-map* technique has been extensively used to understand the workability of many materials. The technique is developed on the basis of dynamic materials modelling (DMM) and the detailed description of the model has been given by Prasad et al. [14, 15].

Experimental

Mg – 3 wt.% Sn – 2 wt.% Ca – 0.4 wt.% Al (TX32 – 0.4Al) alloy was prepared using 99.99% pure Mg, 99.96% pure Sn, 98.5% pure Ca and 99.9% Al. The molten alloy at about 720 °C was kept under a protective cover of Ar+3% SF_6 gas before casting in a pre-heated permanent mold to obtain cylindrical billets of 100 mm diameter and 350 mm length. Cylindrical specimens of 10 mm diameter and 15 mm height were machined from the as-cast billet for compression testing. A 1 mm diameter hole was machined at mid height of the specimen to reach its centre for inserting a thermocouple to measure the specimen temperature as well as the adiabatic temperature rise during deformation.

The data for developing processing maps were obtained from isothermal uniaxial compression tests conducted at constant true strain rates in the range 0.0003 – 10 s^{-1} and temperature range 300 – 500 °C using a computer controlled servo-hydraulic testing machine. Details of the test set-up and procedure are described in an earlier publication [16]. Constant true strain rates during the tests were achieved using an exponential decay of actuator speed in the servo hydraulic machine. Graphite powder mixed with grease was used as the lubricant between the specimen and the compression platens in all the experiments. The specimens were deformed up to a true strain of about 1.0 and then quenched in water. The load - stroke data were converted into true stress - true strain curves using standard equations. The flow stress values were corrected for the adiabatic temperature rise at different temperatures and strain rates and this correction was less important at lower strain rates and higher temperatures. The deformed specimens were sectioned in the center parallel to the compression axis and the cut surface was mounted, polished and etched for metallographic examination. Selected samples were prepared for EBSD by grinding with 320 grit SiC paper, oil based diamond polishing 9, 3, and 1 μm and then vibratory polished followed by cleaning with methanol and ultrasonic cleaner.

The texture of the selected area of the deformed samples was examined using a JEOL 5600 SEM equipped with a NordlysF EBSD detector, and HKL Channel 5 software was used for data collection. EBSD was performed at 20KV, 18-20 mm working distance, a tilt angle of 70° and a scan step size of 2 μm. The portion of the target area that was indexed varied between 75% and 85%. Output texture data is shown as pole figures, in which the horizontal axis of the figure is the compression direction.

Results and Discussion

Processing Map

The processing map of Mg-3Sn-2Ca-0.4Al alloy obtained at a strain of 0.5 is shown in Figure 1 which exhibits two domains of dynamic recrystallization (DRX) in the temperature and strain rate ranges given as follows: (1) 300–350 °C and 0.0003–0.001 s^{-1} with a peak efficiency of 43% occurring at 300 °C and 0.0003s^{-1}, and (2) 400–500 °C and 0.005–0.6 s^{-1} with a peak efficiency of 39% occurring at 450 °C and 0.03 s^{-1}. The higher strain rate diagonal region starting from 300 °C / 0.001 s^{-1} and ending at 470 °C/10 s^{-1} represents flow instability.

The strain rate sensitivity (m) and stress exponent (n) values obtained at the temperature of 500 °C were 0.22 and 4.54 respectively, and the apparent activation energy was 175 KJ/mole in the lower strain rate regime and 195 KJ/mole in the higher strain rate regime [16,17]. It is expected that decrease in flow stress with increase in temperature causes the change in rate controlling process as well as the dominant slip systems.

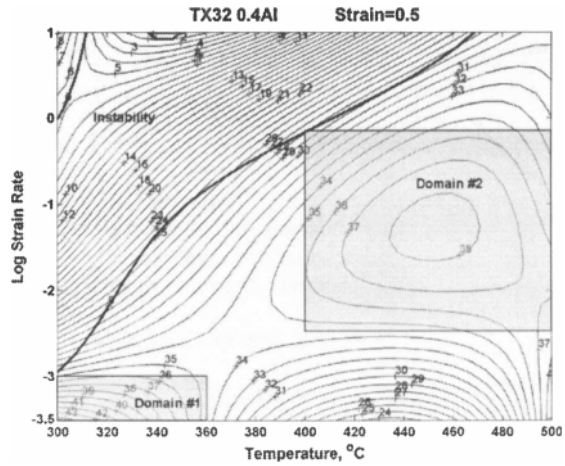

Figure 1. Processing map for Mg–3Sn–2Ca–0.4Al alloy. The numbers against the contours represent efficiency of power dissipation in percent.

Microstructures

The optical microstructures recorded on the specimens deformed in the DRX domain #1 at 300 °C / 0.0003 s^{-1} and 350 °C / 0.001 s^{-1} are shown in Figure 2(a) and (b).

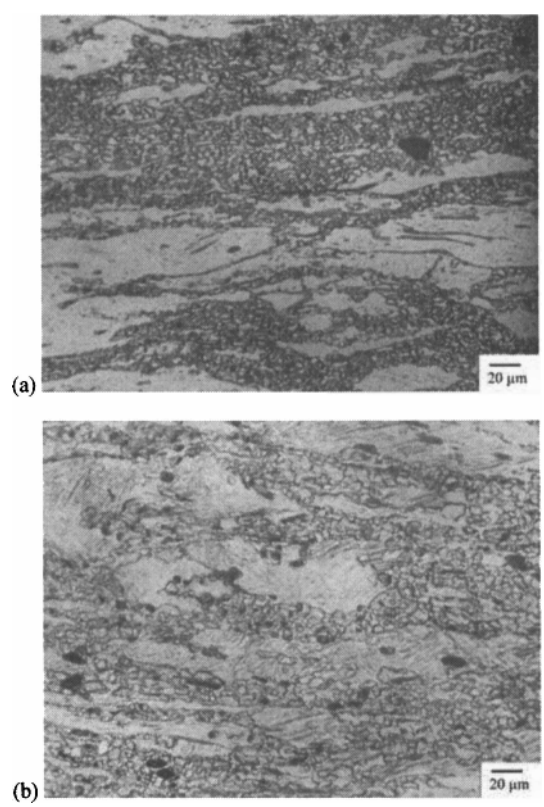

Figure 2. Microstructures of Mg–3Sn–2Ca–0.4Al alloy deformed at (a) 300 °C / 0.0003 s^{-1} and (b) 350 °C / 0.001 s^{-1} (domain #1). Compression axis is vertical.

Both these microstructures indicate that the initial as-cast microstructure is partially converted into fine grained necklaced type of microstructure through a mechanism involving DRX. The optical microstructures of the specimens deformed in the DRX domain #2 at 450 °C / 0.01 s^{-1} and 500 °C / 0.1 s^{-1} are shown in Figure 3(a) and 3(b) respectively. The microstructures were influenced by the deformation conditions. In both the cases, initial as-cast microstructure has transformed into wrought microstructure and all the grains are completely recrystallized. Grain size increased with increase in deformation temperature.

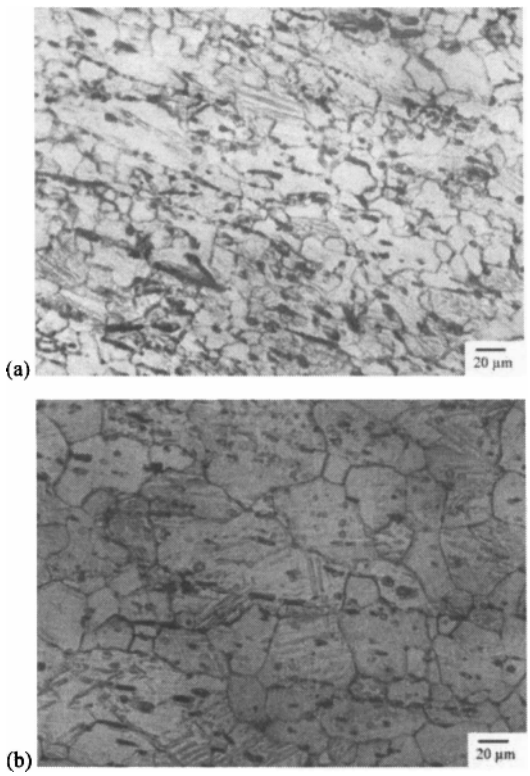

Figure 3. Microstructures of Mg–3Sn–2Ca–0.4Al alloy deformed at (a) 450 °C/0.01 s^{-1} and (b) 500 °C/0.1 s^{-1} (domain #2). Compression axis is vertical.

Texture Evolution

The important slip systems that operate in magnesium materials are: (1) Basal slip (0001) $<11\bar{2}0>$, (2) Prismatic slip $(10\bar{1}0)$ $<11\bar{2}0>$, (3) first order pyramidal slip $(10\bar{1}1)$ $<11\bar{2}0>$ and $(10\bar{1}2)<11\bar{2}0>$, (4) second order pyramidal slip $(11\bar{2}2)<11\bar{2}\bar{3}>$. They get activated when the critical resolved shear stress (CRSS) exceeds relevant threshold levels. During the room temperature deformation of magnesium, basal slip plays the dominant role as it has the lowest CRSS. Prismatic slip becomes extensive at temperatures higher than 225 °C and pyramidal slip system contributes significantly at temperatures higher than 350 °C. As for CRSS, the second easiest slip system is prismatic slip system for Mg alloys. Even the combination of basal and prismatic slip systems is not sufficient to cause large plastic deformation. Among the other slip systems reported for Mg, the second order pyramidal slip system also gets active.

Figure 4 shows pole figures for the Mg-3Sn-2Ca-0.4Al in the as-cast condition and the alloy exhibited near random crystallographic texture.

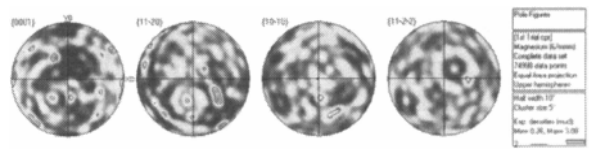

Figure 4. Pole figure corresponding to Mg-3Sn-2Ca-0.4Al alloy in as-cast condition.

Figure 5 shows pole figures for the specimens compressed at 300 °C / 0.0003 s^{-1} and 350 °C / 0.001 s^{-1}. If the original grains in the compressed specimens have their basal planes oriented perpendicular to the compression direction, crystallographic orientation in that position is unfavorable for basal slip. However, fine DRX grains have their basal planes inclined to the compressive direction that favors basal slip. From the pole figure of (0001) in Figure 5(a), it can be noticed that basal poles are spread around 15-30° to the compression direction which makes the crystallographic orientation in the position somewhat favorable for basal slip. The point to note here is the textures of the compressed specimens showed in Figure 5 are the combination of two types of crystallographic orientations with respect to the basal planes of DRX (necklaced) grains and the matrix grains.

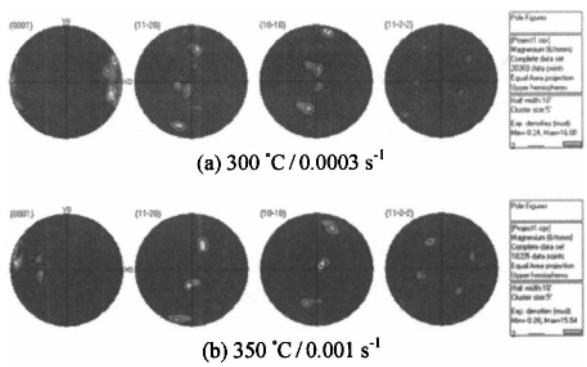

Figure 5. Pole figures corresponding to (a) 300 °C / 0.0003 s^{-1}, (b) 350 °C / 0.001 s^{-1} (domain #1 and X-axis is compression axis).

Maximum frequencies or activation of (0001) $<11\bar{2}0>$ basal slip for the specimens compressed at 300 °C/0.0003 s^{-1} and 350 °C / 0.001 s^{-1} are found to be at Schmid factor values of 0.41 and 0.48 respectively (shown in Figure. 6(a)). Intensity of texture is almost same in both the conditions. From the pole figures of $(10\bar{1}0)$, it can be observed that prismatic slip planes are mostly aligned perpendicular to compressive direction and also rotated by about 10-15° towards compressive direction. As shown in Figure 6(b), high frequency of activation for the prismatic plane through Schmid analysis is found at only 0.02 and 0.04 for the samples deformed at 300 °C / 0.0003 s^{-1} and 350 °C / 0.001 s^{-1} respectively. These low Schmid factor values for prismatic slip indicate that this slip system is not favorably oriented in the used configuration. Even if the stress level is high enough to initiate the prismatic slip, the resolved shear stress in prismatic planes is practically zero due to new grain orientation. At this point, strain

along the c-axis cannot be accommodated during the deformation. The results indicate that by increasing the deformation temperature from 300 °C to 350 °C, basal slip occurs extensively which reorients the basal poles parallel to the compression axis pushing the prismatic poles to become normal to the compression direction. Thus, prismatic slip becomes unfavorable for further deformation.

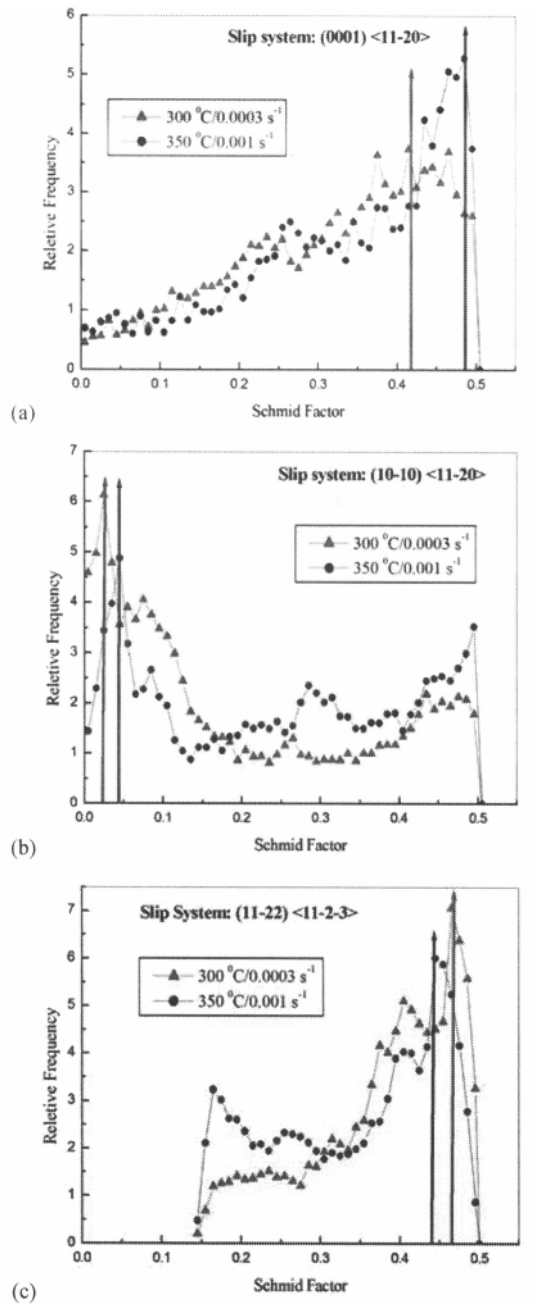

Figure 6. Schmid factor distributions of the grains in the samples deformed at 300 °C / 0.0003 s^{-1} and 350 °C / 0.001 s^{-1} for slip systems (a) basal (b) prism and (c) pyramid slip.

When the flow stress reaches CRSS for pyramidal <c+a> slip, dynamic recrystallization occurs, reducing the density of dislocation tangles and restoring the ductility to the material. To compensate the imposed deformation, <c+a> pyramidal slip is needed and in fact, 2nd order pyramidal system is favorably oriented for the chosen deformation geometry with high Schmid factors of 0.46 and 0.44 for conditions 300 °C / 0.0003 s^{-1} and 350 °C / 0.001 s^{-1} respectively and it is evidenced from Figure 6(c).

The two DRX domains exhibited in the map are separated by 40 °C and it can be viewed as change-over region. Pole figure of the sample deformed at 400 °C / 0.1 s^{-1} is shown in Figure 7. For this condition, texture sharpness was decreased compared to the deformed conditions from domain#1 and this can be attributed to due to the difference in operating slip systems. Prismatic slip also contributed during the deformation of compressed specimen for the said condition. However, with further deformation or with increase in strain, other slip modes take over the deformation causing a shift in the maximum pole density of texture towards <0001> pole (i.e. the c-axis in the grains rotated towards the compressive direction).

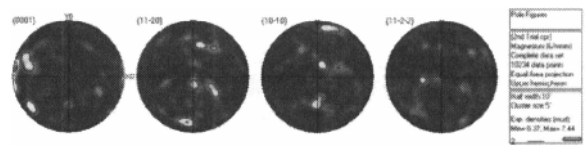

Figure 7. Pole figures corresponding to the deformed condition 400 °C / 0.1 s^{-1}

Texture Randomization (Domain #2)

The pole figure for the specimen deformed at 450 °C / 0.1 s^{-1} is shown in Figure 8. The maximum in the band is laid parallel to compression direction although the planes are split and rotated. $(10\bar{1}0)$ prismatic slip planes are also split and randomized. The geometrical condition for the slip systems is changing with deformation conditions. Similar to the analysis for specimens in domain #1, an analysis on slip systems considering Schmid factors has also been considered for the domain #2 samples. Figure 9 shows the EBSD orientation images for the sample deformed at 450 °C and 0.1 s^{-1} with Schmid factor considerations for basal slip system $(0001)<11\bar{2}0>$ (Figure 9(a)) and 2nd order pyramidal slip system $(11\bar{2}2)<11\bar{2}\bar{3}>$ (Figure 9(b)). It can be seen that high to moderate (red and green colors or dark and light regions marked as A and B respectively) values of Schmid factors dominate the entire images, implying favorable conditions for basal and pyramidal slip systems to operate under this deformation condition.

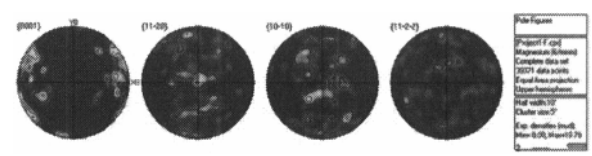

Figure 8. Pole figures corresponding to the deformed condition 450 °C / 0.1 s^{-1}

The pole figures for the specimens deformed at 500 °C / 0.01 s^{-1} and 500 °C / 0.1 s^{-1} are shown in Figure 10. The obtained texture evolution demonstrated that with increase in temperature

and strain rate progressively texture was randomized. This can be attributed to the dominance of slip on (11 $\bar{2}$ 2) pyramidal planes and to the cross-slip associated with the softening process. This is because of the high stacking fault energy (SFE) on pyramidal slip systems (173 mJ/m^2) [18] compared to that on the basal slip systems (60-78 mJ/m^2) [19].

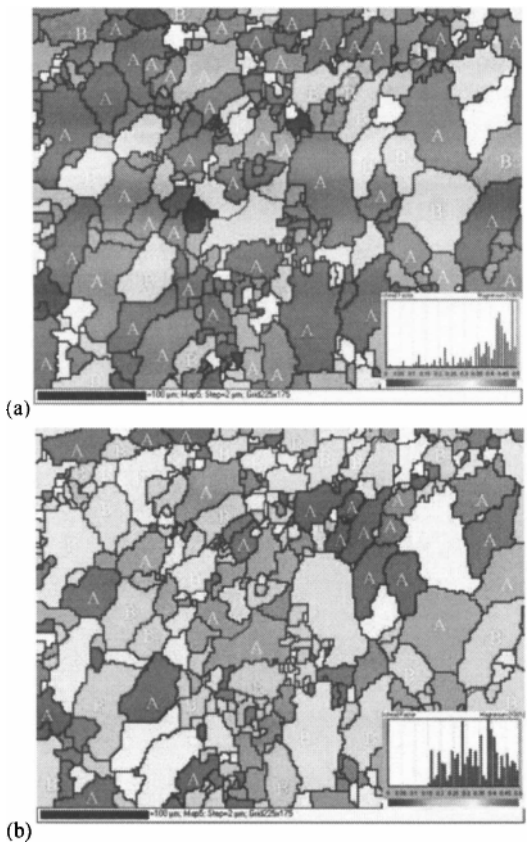

Figure 9. EBSD Schmid factor distribution maps for the sample deformed to 450 °C/0.1 s^{-1} (a) for (0001) <11 $\bar{2}$ 0> slip system (b) for (11 $\bar{2}$ 2) <11 $\bar{2}$ $\bar{3}$ > slip system. The red and green colors or dark and light regions marked as A and B represent high to moderate Schmid factors.

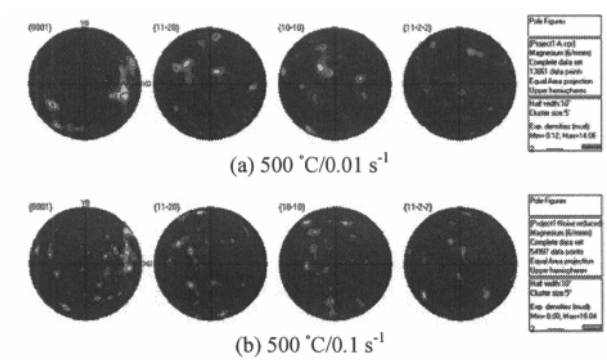

Figure 10. Pole figures corresponding to conditions (a) 500 °C / 0.01 s^{-1} and (b) 500 °C / 0.1 s^{-1}

Summary and Conclusions

Isothermal uniaxial compression tests were performed on as-cast Mg-3Sn-2Ca-0.4Al alloy to study the effect of deformation conditions on microstructure and texture evolution. The main results are summarized as follows:

(1) Occurrence of the dynamic recrystallization was confirmed by microstructure observation and texture evolution.
(2) The strain rate and temperature have significant influence on the microstructure and texture evolution during uniaxial compression of Mg-3Sn-Ca-0.4Al alloy.
(3) Most basal planes are aligned 15-30° to the compression direction at relatively low temperature (300 °C, 350 °C) and low strain rate (0.0003 s^{-1}, 0.001 s^{-1}). Texture is randomized at higher temperature (500 °C) and higher strain rate (0.1 s^{-1}).
(4) All the three slip systems <a> basal, <a> prismatic, <c + a> pyramidal are necessary for the accommodation of deformation of Mg-3Sn-2Ca-0.4Al alloy. <c + a> pyramidal slip is of crucial importance for achieving high workability.
(5) The optimized condition for hot working of Mg-3Sn-2Ca-0.4Al alloy is 500 °C/0.1 s^{-1}.

Acknowledgement

This work was supported by a grant (Project #115108) from the Research Grants Council of the Hong Kong Special Administrative Region, China.

References

1. A.A. Luo, "Recent magnesium alloy development for elevated temperature applications", *International Materials Reviews*, 49 (2004), 13-30.

2. B.C. Wonsiewicz and W.A. Backofen, "Plasticity of Magnesium Crystals", *Trans Metall Soc AMIE*, 239 (1967), 1422-1431.

3. C.S. Roberts, *Magnesium and its alloys* (John Wiley and Sons, New York, NY, 1960), 180.

4. R.E. Reed-Hill and W.D. Robertson, "The Crystallographic Characteristics of Fracture in Magnesium Single Crystals", *Acta Metall*, 5 (1957) 728-737.

5. W. Hosford and R.M. Caddle, *Metal forming: Mechanics and Metallurgy*, (Prentice-Hall, 1993), 43-44.

6. W. Hosford, *The Mechanics of Crystals and Textured Polycrystals* (New York: Oxford University Press, USA, 1993), 122-124.

7. E. Schmid and W. Boas, *Plasticity of Crystals: With special reference to Metals* (London: Chapman and Hall, 1935), 140-141.

8. J.A. Chapman and D.V. Wilson, "The room-temperature ductility of fine-grain magnesium", *J Inst Met*, 91 (1962), 39-40.

9. J. Koike, "The activity of non-basal slip systems and dynamic recovery at room temperature in fine-grained AZ31B magnesium alloys", *Acta Mater*, 51 (7) (2003), 2055-2065.

10. T. Abu Leil et al., "Corrosion Behavior and Microstructure of a Broad Range of Mg-Sn-X Alloys," *Magnesium Technology 2006*, eds. A.A. Luo, N.R. Neelameggham and R.S. Beals (Warrendale, PA: The Minerals, Metals and Materials Society, 2006), 281-286.

11. T. Abu Leil et al., "Effect of Heat Treatment on the Microstructure and Creep Behavior of Mg-Sn-Ca Alloys," *Mater Sci Forum*, 546-549 (2007), 69-72.

12. T. Abu Leil et al., Development and Charecterization of a series of Mg-Sn-Ca Alloys, in: *Magnesium Technology in global age*, eds. M.O. Oekguleryuz and L.W.F. Mackenzie, COM 2006, Montreal, Canada, 2006, 739-749.

13. K.M. Asl, A. Tari, and F. Khomamizadeh, "The Effect of Different Content of Al, RE and Si Element on the Microstructure, Mechanical and Creep Properties of Mg-Al Alloys," *Mater Sci Eng*, A523 (2009), 1-6.

14. Y.V.R.K. Prasad et al., "Modeling of dynamic material behavior in hot deformation: Forging of Ti-6242", *Metall Trans*, 15A (1984), 1883-1892.

15. Y.V.R.K. Prasad and T. Seshacharyulu, "Recent advances in the science of mechanical processing", *Indian J Technol*, 28 (1990), 435-451.

16. K.P.Rao, Y.V.R.K. Prasad, N. Hort, K.U. Kainer, "Effect of aluminum addition on the strengthening and high temperature deformation bahavior of Mg-3Sn-2Ca alloy", *Magnesium Technology 2010*, eds. S.R. Agnew, N.R. Neelameggham, E.A. Nyberg and W.H. Sillekens (The Minerals, Metals and Materials Society, 2010), 201-205.

17. K.P. Rao, Y.V.R.K. Prasad, C. Dharmendra, N. Hort, K.U. Kainer, "Compressive strength and hot deformation behavior of TX32 magnesium alloy with 0.4% Al and 0.4% Si additions", *Mater Sci Eng*, A528 (2011), 6964-6970.

18. J.R. Morris, J. Scharaff, K.M. Ho. D.E. Turner, Y.Y. Ye, M.H. Yoo, "Prediction of a {11-22} hcp stacking fault using a modified generalized stacking-fault calculation", *Phil Mag*, 76 (1997), 1065-1077.

19. D.H. Sastry, Y.V.R.K. Prasad and K.I. Vasu, "On the stacking fault energies of some close-packed hexagonal metals", *Scripta Metall*, 3 (1969), 927-930.